[redacted]

GPO PRICE $ _____

CFSTI PRICE(S) $ _____

Hard copy (HC) 2.00

Microfiche (MF) .50

ff 653 July 65

[redacted]

WYLE LABORATORIES

TESTING DIVISION, HUNTSVILLE FACILITY

FACILITY FORM 602

N66 30316 (ACCESSION NUMBER)	(THRU)
48 (PAGES)	1 (CODE)
CR-76126 (NASA CR OR TMX OR AD NUMBER)	12 (CATEGORY)

research

WYLE LABORATORIES - RESEARCH STAFF
Report WR 66-23

FLOW VISUALIZATION EXPERIMENTS WITH SEPARATED SUPERSONIC TURBULENT FLOW

by

M. V. Lowson

Work performed under Contract NAS8-11308

Prepared by M. V. Lowson
M. V. Lowson

Approved by L. C. Sutherland
L. C. Sutherland

Approved by Kenneth McK. Eldred
Kenneth McK. Eldred
Director of Research

April, 1966

COPY NO. 16

SUMMARY

30316

Shadowgraph and surface flow visualization experiments have been performed on a cylinder-flare-cylinder half model mounted on the wall of a seven inch supersonic wind tunnel. The object of the experiments was to define the geometry and flow mechanisms of turbulent supersonic separations. The results generally support earlier analyses of the flow. It has also been shown that the reattachment process is unsteady, and must be expected to lead to substantial fluctuating surface loadings on the flare. The mean reattachment point was found to move up the flare with increase in flare angle, and its height was found to be an approximately constant proportion of the step height. It also appears that the separation geometry on space vehicles will be significantly affected by the presence of the escape tower and surface protuberances.

TABLE OF CONTENTS

LIST OF TABLES

LIST OF FIGURES

LIST OF FIGURES (Continued)

1.0 INTRODUCTION

Current space vehicles, particularly large multistage launch vehicles, are typified by abrupt changes in external contour. These sudden changes give rise to extensive regions of separated flow, immediately behind the shoulders at subsonic and transonic speeds, and in front of the flares at supersonic speeds. Such regions of separated flow can have significant effects on the aerodynamic characteristics of the vehicle, both on the stability and control, and on the fluctuating loadings applied to the surface. It is known that a number of vehicles have undergone catastrophic failure while under the action of these fluctuating loadings.

However, at the present time there is insufficient knowledge even to allow the mean characteristics of such separated flows to be predicted with confidence. Previous experimental and theoretical studies have been aimed at the suppression of separation, so that data on fully developed separated flows is fragmentary. An analysis of the available data was presented in Reference 1, where it was suggested that the supersonic separated flows could be split into three types. These three types are shown in Figure 1. It was suggested in Reference 1 that the key parameter affecting the geometry of the separation region was the position of the reattachment point. In Figure 1, type A corresponds to a reattachment point on the flare surface while types B and C have the reattachment point at, or near, the shoulder. For the type A flow to exist, the angle of the flare must be less than the critical angle at the free stream Mach number, and it would be anticipated that the size of the separation region would be proportional to the upstream boundary layer thickness. If the flare height is less than the natural size of the separation region, it was postulated that type B flow (see Figure 1) would occur, and flows with angles above the critical angle would be expected to give type C flows.

Each of these flows has been observed in wind tunnel experiments. The type A flows were studied in detail by Kuehn (Reference 2) and types B and C flows may be observed in many shadowgraphs. However, it is extremely difficult to predict which flow will occur for any given geometry, particularly for moderate flare angles. There is very little data which can be applied to give criteria which will distinguish between type A and B flows, and although the approximate critical flare angle for any given Mach number can be obtained from Tables (Reference 3), it is unlikely that the complex flows actually accompanying the reattachment region can be accurately modeled by the simple two-dimensional or conical flows given therein.

The need for further experimental work is clear, and the present experiments involved shadowgraph and surface oil flow visualization on a cylinder flare-cylinder half model mounted on the wind tunnel wall. High speed schlieren motion pictures were also made. The object of the experiments was to obtain data on the separation geometry, and to give further information on mechanisms underlying supersonic turbulent separated flows. In particular, the data obtained was intended to assist in accurate prediction of the mean flow for typical launch vehicle geometries.

2.0 APPARATUS

The experiments were performed in the Marshall Space Flight Center seven inch supersonic wind tunnel, which is described more fully in Reference 4. A list of the leading characteristics of the wind tunnel is presented as Table 1. In Reference 1, it was suggested that Reynolds number has a critical effect on the test results and that a Reynolds number based on boundary thickness greater than 8×10^4 was desirable. The Reynolds number per foot of the seven inch tunnel is low since the stagnation pressure is atmospheric and analysis, presented in Reference 5, showed that under the criterion above neither axisymmetric or two dimensional models would be suitable for the present tests. Therefore, a semicircular section half model mounted on the wind tunnel wall was adopted. Data from Reference 6 showed that the wall boundary layer was sufficiently thick to allow the criterion above to be met at least for some cases, as shown in Table 2.

The model configuration was a cylinder flare-cylinder, and it was positioned so that the estimated separation point was a constant eight inches in front of the nozzle trailing edge. The basic semi-cylinder was 1 inch in diameter and was faired into the nozzle liner so that the top surface was parallel to the wind tunnel axis (see Figure 2). Four faired cylinders were made to fit the nozzles for the four Mach numbers used in the tests. Any gaps between model and nozzle liner were faired in with putty. A range of four step heights was chosen; 0.3, 0.6, 1.2, and 2.4 inches, corresponding approximately to 1, 2, 4, and 8 boundary layer thicknesses, and flares were constructed with six angles; 15, 20, 30, 45, 60, and 90 degrees. However, the 2.4 inch step height models succeeded in blocking the tunnel in nearly all cases, so that useful results are limited to the models with the first three step heights mentioned above. A listing of the model dimensions may be found in Table 3. In order to attach the models to the tunnel, the 0.3 inch step height flares had to be enlarged at the rear. Therefore, for these 0.3 inch models a second flare was provided with identical dimensions to the first. The second flare was positioned 6.75 inches behind the first.

Shadowgraph visualization of the flow was made, using a simple spark source of approximately 1 microsecond duration, the film being placed immediately next to the tunnel window in a special frame. The spark source was placed in line with the shoulder of each model so that the 90° flare models would record correctly. Previous shadowgraph experiments in this tunnel had shown that adequate definition was not obtained at the highest Mach numbers, due to low flow density. Thus, the Mach numbers chosen for this test were 1.59, 1.99, 2.49, and 2.94, each Mach number requiring the insertion of a special nozzle liner in the wind tunnel. A listing of the conditions for each run appears as Table 4. This may be used for the identification of shadowgraph and surface flow pictures. Note that the Mach numbers here are probably accurate only to $\pm$ 3 percent.

Two methods of surface flow visualization were evaluated. The initial technique used a suspension of fluorescent pigment in oil, and the surface flow patterns were photographed using ultraviolet light. In spite of considerable variation in oil viscosity, pigment density and other parameters, it was found that the definition of the surface flow patterns using this method was inadequate. It was found that a better technique was to use a suspension of china-clay in oil of wintergreen. The experiments were

carried out while this mixture was still wet and it was found that this technique gave very clear definition of the surface flow patterns without the complications of ultraviolet lighting and long exposures. In addition this technique enabled the flow patterns to be seen clearly from outside the tunnel, thus allowing a visual check that the flow patterns did not alter during the shut down of the tunnel after each run. It should be emphasized that this technique is not at all similar to the more usual "china-clay" technique used to detect transition to turbulence (Reference 7), and that the flow patterns presented in this report are simply surface flow patterns with no direct relation to transition location.

After each surface flow visualization run, photographs of the interesting flow features were taken. In addition, the distance from the cylinder flare junction to separation and reattachment points was measured. The separation point was normally defined clearly by the surface flow (see Figure 12), although its distance from the junction was not always constant around the model. The reattachment point could usually be identified as a cusp locus (Reference 8, also, see Figure 10), although it was found that confusing results occurred for the 90 degree flare cases.

In order to check the boundary layer thickness on the simple cylindrical model, a pitot rake was constructed. Dimensions for the rake are given in Table 5. For each Mach number, the boundary layer profiles were measured at the anticipated point of separation, eight inches in front of the nozzle trailing edge.

3.0 RESULTS

The principal results of these tests were the shadowgraph and surface flow pictures that were taken. Clearly,it is impractical to reproduce all the photographs in the present report and only a selection appear here. Figures 3 to 8 demonstrate the general form of the shadowgraphs observed in the present experiments. The forward "separation" shock marked the beginning of the separation zone, and some vestige of a "reattachment" shock complex was usually apparent at some position on the flare. These general forms are similar to those sketched in Figure 1. Little overall variation of the shadowgraph pictures was observed with change in Mach number or step height, so that the sequence shown in Figures 3 to 8 may be taken as representative. Note that the parabolic shocks visible on the shadowgraphs represent the intersection of the conical shocks from the model with the window and are not present on the model itself.

The surface flow visualizations (Figures 9 to 12) gave less consistent results, mainly because the visualization obtained was critically dependent on the consistency of the china-clay mixture and on the run time. Many of the surface flow patterns showed standing vortex patterns at the intersection of the model with the wall (as for example in Figure 12). These are not unreasonable, and should not affect the validity of the shadowgraphs or surface flow visualization at the top of the model. Many of the observed surface flow features did not photograph well, and the figures presented here (Figures 9 to 12) have been chosed for their clarity, but are representative of the flows actually observed on the model.

Tables 6 and 7 give the actual measurements of the separation and reattachment lengths from the cylinder flare junction during the surface flow experiments. These measurements are probably accurate to $\pm$ 0.05 inch. Tables 8 and 9 give measurements taken directly from the shadowgraph photographs. The separation length given in Table 8 is the distance from flare junction to the projection of the separation shock on the cylindrical surface. This point is not necessarily the point of separation, and evidence presented below suggests the shock is unsteady, so that an instantaneous recording of the shock position is unlikely to reveal it at its mean position. Within these limitations, the accuracy of the separation length is probably within $\pm$ 0.05 inch. The shock angles in Table 9 refer to the angle of the shock near to the surface. As can be seen from Figure 7, the shocks were not entirely straight and the angles given in Table 9 are expected to be accurate to $\pm$ 1 degree. Since the shadowgraphs were taken in conical light, some distortion was inevitable. However, calculations showed that this distortion was insignificant in the present case, and certainly negligible compared with the other inaccuracies discussed above.

Unfortunately, results from the boundary layer rake were inconclusive because of the small number of tubes actually within the boundary layer. It was clear that the boundary layer thickness was greater than 0.2 inches and less than 0.3 inches in all cases, but the results do not allow any more precise determination of the boundary layer thickness. The results do suggest that the boundary layer was slightly less thick than anticipated.

4.0 DISCUSSION

The surface flow patterns demonstrate that separation is actually occurring in the flare region for angles greater than 30 degrees. Moreover,the separation point indicated by the shock is in broad agreement with that indicated by the surface flow patterns. Other experiments with similar shock patterns have sometimes cast doubt on the existence of separated flow, but the present tests seem reasonably conclusive on this point. Comparison of Tables 6 and 8 also shows that the separation point indicated by the shadowgraphs is generally in front of the separation point measured using the surface flow patterns. It is probable that this is due to the identification of the separation point in the shadowgraph experiments as the intersection of the projected shock and the surface. In reality the separation point would be expected to lie somewhere beneath the intersection of the shock with the outer regions of the boundary layer. Various models for this case were used in an attempt to give a reasonable numerical estimate of this effect, but no model could be found which gave acceptable results for all the data.

Figure 13 gives a plot of the separation length, measured in the surface flow visualization tests, against flare angle. The separation length has been divided by the flare height. Note that points which would have been superimposed have been displaced laterally for clarity. Figure 13 shows how the separation length is an approximately constant proportion of the flare height, for flare angles of 45 degrees and greater. For the 30 degree flare, however, this is not the case. These results are broadly consistent with the arguments put forward in Reference 1. The 30 degrees flare corresponds to a type A flow (see Figure 1) with the separation length being proportional to boundary layer thickness and the 45, 60, and 90 degree flares give type C flows with the separation length proportional to step height.

If the separations can be regarded as "free-interactions" as defined by Chapman, Kuehn and Larson (Reference 9, see also Reference 1) then the angle at which the flow separates from the wall should be constant. Analysis presented in Reference 1 indicated that an angle of 12.5 degrees gave a good approximation to many experimental results. However it appears that an angle of 14 degrees would be more appropriate to the present data. Figure 13 gives a curve showing the separation length against flare angle assuming a separation angle of 14 degrees and reattachment at the shoulder. Examination of Figure 13 shows that the non-dimensionalized separation length reduces consistently with increase in step height. This effect cannot be explained fully, although one contribution to this is the variation in reattachment height discussed below. In general Figure 13 shows that the effect of Mach number on the results is to reduce the separation length at Mach 1.99 and 2.49 compared to Mach 1.59 and 2.94. This effect is similar to that of the results analysed in Reference 1, and has also been observed in unpublished theoretical work performed by the author. This effect is therefore assumed to be real.

It was originally postulated that reattachment occurred at the shoulder for high enough flare angle. However, the results of Table 7 show this is not generally the case. Figure 14 gives a graph of reattachment height, divided by step height, against flare angle.

Figure 14 shows how the reattachment height moves up the flare with increase in flare angle and, for any given angle, is an approximately constant proportion of the step height, at least for the 45 degree and 60 degree cases. Some scatter is apparent for the 30 degree cases. Little consistent effect of either step height or Mach number can be observed in Figure 14.

The results shown for the 90 degree flares in Table 7 are unlikely to correspond to the actual reattachment points. Careful examination of the surface flow patterns for the 90 degree flares generally revealed traces of a reattachment zone very near the top edge of the step, but it was not usually defined sufficiently well to enable measurements to be taken. The measurements for this case shown in Table 7 refer to a clearer marking near the compression corner which can be seen, for instance, in Figure 12. This marking is thought to correspond to a secondary separation zone in the corner, and a sketch of a possible flow pattern for this case is shown as Figure 15. This supposition is supported by some of the shadowgraph pictures of the 90 degree case which also show unusual flow features in the compression corner (for example Figure 16). However, from the present tests it does seem reasonable to suppose that the reattachment point for the primary separation is at, or just below, the shoulder.

The information on reattachment point location given by Table 7 and Figure 14 may be used to extend the constant separation angle hypothesis discussed above. The angle between the surface and the line joining separation and reattachment points has been calculated for the present data and is shown in Table 10. Reattachment for the 90 degree cases has been assumed to be at the shoulder. The figures in Table 10 still show some scatter, but do represent an improvement over those which result from the assumption of shoulder reattachment suggested in Reference 1. A consistent increase in separation angle with step height and flare angle is still apparent in Table 10 but there is no clear effect of Mach number. It should be noted that there is no obvious physical reason for the line between the separation and reattachment points to be entirely straight, and indeed some curvature towards the reattachment point is to be expected. The analysis above, based on straight line criteria, is essentially an engineering approximation.

In general, the results obtained during the present experiments for the 30 degree case do not admit any clear interpretation. It had been hoped that they would show either clear linear dependence or independence on step height. However, the actual results for the 30 degree flare show a minor increase in separation length with increase in step height at all Mach numbers. The separation lengths decrease slightly at the highest Mach numbers. Thus the present results offer no support for either of the hypothesis advanced above and, in particular, do not support the tentative analysis in Figure 9 of Reference 1.

Negligible separation was observed for the 15 and 20 degree flare cases, but the form of the shadowgraphs for these cases is of interest. Figure 4 shows how the shock wave is followed by an area of markedly increased turbulence. The appearance of the shadowgraphs may be explained following a theoretical analysis by Ribner (References 10 and 14). Ribner showed that turbulent velocity fluctations passing through a shock are transformed into turbulent pressure and entropy fluctuations. Turbulent pressure fluctuations are directly linked to the density fluctuations which record on a shadowgraph.

Thus, unrecorded velocity fluctuations before the shock will transform into very clear density fluctuations after passing through the shock. It is thought that this effect explains the appearance of Figure 4. This is of some practical importance since the density fluctuations must themselves be associated with important fluctuating pressure loadings. Thus, even though the flow remains essentially unseparated, important sources of fluctuating surface loading may still be present.

The drawing of practical conclusions from the present results is complicated by observations on the second shoulder of the 0.3 inch step height flares. Virtually all the shadowgraphs demonstrate increased separation lengths on these flares, typically about 10 percent. These increases appear to be particularly significant on the 20 degree flares. The increase in separation length is presumably due to the increase in turbulence level and the effective boundary layer parameters for the flow approaching the second flare. Therefore, it must be anticipated that the results obtained here cannot be applied directly to the flares on space vehicles since the numerous appendages; e.g. the escape tower, on a modern space vehicle will inevitably cause similar increases in turbulence level and boundary layer thickness.

Unfortunately there are no results which relate the numerical magnitude of this increase to any flow characteristic and its full significance is unknown. However it may be noted that theoretical investigations (References 12 and 13) have demonstrated the importance of the "form parameter" H, given by dividing the boundary layer displacement thickness by the momentum thickness. Increases in the value of H correspond to development of the boundary layer towards separation, and also to reduction in the separation angle. Physically this means that the closer a boundary layer is to separation, the further forward the separation imposed by the flare can travel. Previous investigators have not recorded values of H during their experiments, and measurements in the pres ent tests were not possible because of the very limited number of points actually obtained within the boundary layer with the pitot rake. Thus, the effect of form parameter and other boundary layer characteristics must remain conjectural, but is recommended as a valuable future study.

During the first experiments only one shadowgraph picture was taken at each condition, but examination of these shadowgraphs showed a surprising lack of uniformity in the flow patterns. Thus, a number of shadowgraphs of the same condition were made to check on the steadiness of the flow in the separation region. It was found that the flow was definitely unsteady, particularly in the reattachment region. Some shadowgraphs showing the extent of this variation are presented here as Figures 16 to 18. Shadowgraph sequences taken for the 1.2 inch step height at 30, 45, and 90 degree flare angles have shown very definite unsteadiness, and there can be little doubt that this unsteadiness exists at all separated conditions.

The most obvious differences between Figures 16 to 18 are within the reattachment region. Attempts have been made to find a logical sequence for the shadowgraphs recorded, so that some broad features of an unsteady mechanism could be defined. There is some evidence of a growing corner disturbance, possibly an unsteady secondary separation (see Figure 15). This effect may be observed in the sequence of Figures 16 to 18.

Alternatively this may be regarded as an effect of a moving reattachment shock, but unfortunately the evidence is inconclusive. High speed schlieren motion pictures of various cases have also been made, but unfortunately little detail was apparent in the reattachment region. However,these motion pictures did demonstrate significant unsteadiness in the separation shock, which seemed to move in a random manner with occasional excursions along the surface of up to a boundary layer thickness. It has recently been suggested that shock-turbulence interaction could be responsible for the observed fluctuating pressure loading beneath the separation shock (Reference 14) and the results from these experiments do not cast doubt on this possibility. However, the experiments do show that random shock impingement is a probable cause of pressure fluctuations on the flare in the reattachment region. Note, however, that the fact that surface flow visualization of the reattachment line was possible does demonstrate that some order is preserved in the mean flow. Experimental work on the unsteady aspects of the experiments is continuing.

5.0 CONCLUSIONS

Shadowgraph and surface flow visualization experiments have been performed on a series of cylinder-flare-cylinder half models mounted on the wall of the Marshall Space Flight Center seven inch supersonic tunnel. These experiments have supported the broad features of separated flows put forward in Reference 1. In detail it is concluded that:

1. The separation length is an approximately constant proportion of the step height for flare angles of 45 degrees and above.
2. Negligible separation is apparent for flares of 20 degrees and less.
3. The intense turbulence observed behind the shock at these small angles is a result of the conversion of turbulent velocity fluctuations to turbulent density fluctuations by the shock.
4. The flare reattachment point moves up the flare with increase in flare angle.
5. The reattachment height is an approximately constant proportion of the step height for flares of 45 degrees and greater.
6. The line joining the separation and reattachment points lies at an angle to the surface between 12 degrees and 15 degrees independent of flare angle.
7. The separation shock is unsteady with occasional excursions along the surface of up to one boundary layer thickness.
8. The reattachment shock complex is entirely unsteady, and random shock impingements must be expected to give high levels of fluctuating pressures on the flare.
9. Flares subsequent to the first, or behind the escape tower or surface protuberances, are expected to exhibit larger regions of separation.

The following recommendations for future work are put forward:

1. Further data on reattachment is required from surface flow visualization experiments.
2. It is desirable to repeat the present experiments in a larger tunnel to ensure that Reynolds numbers are sufficiently high. Results from two dimensional and axisymmetric models are also required.
3. Experiments to define the significance of upstream boundary layer characteristics on separation phenomena are desirable.

4. Supporting theoretical work on the above problem will be required.

5. Further experiments to define the unsteady flow processes within the separation region appear most valuable.

6. Detail measurements of the fluctuating surface pressures on a series of flares are desirable to define the significance of reattachment shock impingement, and also to define the magnitude of the anticipated loadings in the unseparated cases.

ACKNOWLEDGEMENTS

The experimental program was executed by the staff of the Marshall Space Flight Center wind tunnel facility under the direction of L.A. Schutzenhofer of the Marshall Space Flight Center, and D.E. Shelor of Northrop Space Laboratories.

REFERENCES

1. Lowson, M. V., The Acoustic Environment Due to Separated Flows and Oscillating Shocks, Wyle Research Report WR-66-8, March 1966.

2. Kuehn, D. M., Turbulent Boundary Layer Separation Induced by Flares on Cylinders at Zero Angle of Attack, NASA TR-117, 1961.

3. Ames Research Staff, Equations Tables and Charts for Compressible Flow, NACA Rep 1135, 1953.

4. Cope, D. O., Calibration Test Results of Various Supersonic Nozzles in the Redstone 7 x 7 inch Wind Tunnel, Aeroballistics Internal Note 173, February 1957.

5. Lowson, M. V., Supersonic Turbulent Separation Tests in the Marshall Space Flight Center 7 inch Tunnel, Wyle Research Staff TM-65-4.

6. Butler, M. G. and Simmons, C. W., Boundary Layer Calibration of the George C. Marshall Space Flight Center's 7 x 7" Bi-sonic Wind Tunnel, Wind Tunnel Note 107, August 1964.

7. Richards, E. J., Burstall, F. H., The "China-Clay" Method of Indicating Transition, British A.R.C., R M 2126, 1945.

8. Maskell, E. L., Flow Separation in Three Dimensions, British A.R.C., Rep 18,063, 1955.

9. Chapman, D. R.; Kuehn, D. M.; and Larson, H. K., Investigation of Separated Flows in Supersonic and Subsonic Streams with Emphasis on the Effect of Transition, NACA Rep 1356, 1958.

10. Ribner, H. S., Correction of a Pattern of Volicity Through a Shock Wave, NACA Rep 1164, 1954.

11. Ribner, H. S., Shock-Turbulence Interaction and the Generation of Noise, NACA Rep 1233, 1955.

12. Schuh, H., On Determining Turbulent Boundary Layer Separation in Incompressible and Compressible Flow, J.Ac. Sci. Vol. 22, pp 343-345, May 1955.

13. Mager, A., Prediction of Shock-Induced Turbulent Boundary Layer Separation, J.Ac.Sci. Vol. 22, pp 201-202, March 1955.

14. Lowson, M. V., Preliminary Results for Near Field Pressures Due to Shock Interactions, Wyle Laboratories Quarterly Progress Report for October, November and December 1965, on Contract NAS8-11308.

TABLE 1

AERODYNAMIC CONSTANTS FOR THE MARSHALL SPACE FLIGHT CENTER SEVEN INCH TUNNEL

MACH NO	1.54	1.99	2.44	3.00	3.26	4.00	5.00
MASS FLOW (LB/SEC)	13.053	10.030	6.382	3.686	2.802	1.392	0.576
DYNAMIC PRES. (PSI)	6.26	5.29	3.94	2.52	2.03	1.08	0.486
STATIC PRES. (PSI)	3.78	1.91	0.945	0.400	0.272	0.097	0.028
MACH ANGLE (DEG)	40° 30'	30° 10'	24° 12'	19° 28'	17° 52'	14° 29'	11° 32'
LENGTH OF TEST RHOMBUS (IN.)	8.871	12.913	15.985	19.395	22.495	27.100	35.571
TEST SECTION HEIGHT (IN.)	7.150	7.380	7.184	6.856	7.250	7.000	7.260
THROAT OPENING (IN.)	5.522	4.250	2.694	1.560	1.186	0.592	0.236
LENGTH OF NOZZLE (IN.)	8.831	16.750	13.625	15.125	16.304	19.636	20.506
LENGTH OF MODEL (IN.)	6.421	9.523	10	10	10	10	10
REYNOLDS NO/IN.	360,353	305,185	250,000	185,608	163,971	111,306	82,216
MINIMUM STARTING PRESSURE (PSIA) (TUNNEL CLEAR)	10.6	9.25	6.55	5.41	5.01	1.65	0.75
MAXIMUM RUN TIME (SEC)	183	210	225	332	379	425	391

ATMOSPHERIC CONDITIONS $P = 14.7$ PSIA, $T = 90^{\circ}F$, $\rho = 0.0722$ LB/FT^3

From Initial Tunnel Calibration in Reference 4.

TABLE 2

UNDISTURBED BOUNDARY LAYER CHARACTERISTICS AT SEPARATION POINT

Mach Number	1.59	1.99	2.49	2.94
Approximate Boundary Layer Thickness (inches)	0.2	0.31	0.33	0.33
Reynolds Number based on Boundary Layer Thickness	7.2×10^4	9.5×10^4	8.3×10^4	6.6×10^4

Data from References 4 and 6.

TABLE 3

MODEL DIMENSIONS IN INCHES

Step Height		0.3	0.6	1.2	2.4
External Radius		0.8	1.1	1.7	2.9
Length of flare from shoulder to front of Model	15°	1.120	2.239	4.477	8.957
	20°	0.824	1.649	3.297	6.594
	30°	0.520	1.039	2.079	4.157
	45°	0.3	0.6	1.2	2.4
	60°	0.173	0.346	0.693	1.386
	90°	0	0	0	0
Distance Shoulder to rear of Model		12.75	11.75	9.5	5.0
Thus distance of shoulder in front of Nozzle T.E.		6.75	5.75	3.5	-1.0

TABLE 4

MODEL CONDITION FOR EACH RUN NUMBER

Mach Number	Step Height	Flare Angle α in Degrees 15	20	30	45	60	90	
1.59	0.3	2	3	4	1	5	6	Shadowgraph
		1	2	3	4	5	6	Surface Flow
	0.6	7	8/0 8/1	9	10	11	12	
	1.2	13	14*					
1.99	0.3	16	17	18	19	20	21	
	0.6	27	26	25	24	23	22	
	1.2	28	29	30	31	32	33	
	2.4	34*						
2.49	0.3	41	40	39	38	37	36	
	0.6	42	43	44	45	46	47	
	1.2	48	49	50	51	52	53	
	2.4	54*						
2.94	0.3	57	58	59	60	61	62	
	0.6	63	64	65	66	67	68	
	1.2	69	70	71	72	73	74	
	2.4	75	76*					

All run numbers except M = 1.57, h = 0.3 apply to both shadowgraph and surface flow experiments.

* denotes tunnel blocked

Runs 15, 35, 55, and 77 were boundary layer probe runs at M = 1.59, 1.99, 2.49, and 2.94 respectively.

TABLE 5

BOUNDARY LAYER RAKE DIMENSIONS

Dimensions taken from body to Center Line of Tube

Tube	Inches
1	0.014
2	0.089
3	0.164
4	0.239
5	0.314
6	0.389
7	0.464
8	0.539
9	0.689
10	1.089
11	1.589
12	2.089

TABLE 6

SEPARATION LENGTHS MEASURED FROM SURFACE FLOW VISUALIZATION EXPERIMENTS

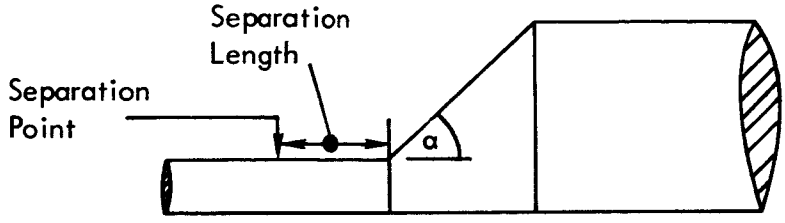

Mach Number	Step Height	Flare Angle α in Degrees 15	20	30	45	60	90	
1.59	0.3	0.18	0.33	0.595	0.875	1.050	0.93	(First Shoulder)
	0.6	-	0.23 0.22	0.85	1.48	1.73	2.14	
	1.2	-	0.1	TUNNEL BLOCKED				
1.99	0.3	0.1	0.23	0.51	0.82	0.91	1.11	(First Shoulder)
	0.6	0.09	0.24	0.58	1.42	1.72	2.22	
	1.2	0.09	0.22	0.78	2.36	3.18	4.08	
2.49	0.3	0.06	0.14	0.5	0.87	1.0	1.2	(First Shoulder)
	0.6	0.04	0.08	0.44	1.42	1.78	1.28	
	1.2	0.04	0.16	0.74	2.66	3.45	4.32	
2.94	0.3	0.07	0.12	0.37	0.72	0.98	1.24	(First Shoulder)
	0.6	0.08	0.14	0.26	1.16	1.68	2.34	
	1.2	0.06	0.16	0.48	2.12	3.32	4.26	
	2.4	0.08	TUNNEL BLOCKED					

Separation Length Measured in Inches

TABLE 7

REATTACHMENT LENGTHS MEASURED FROM SURFACE FLOW VISUALIZATION EXPERIMENTS

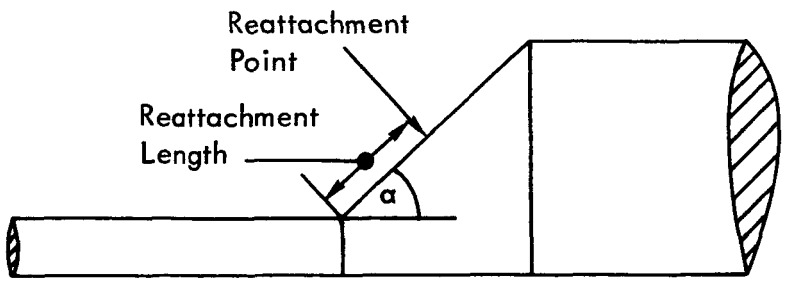

Mach Number	Step Height	Flare Angle α in Degrees 30	45	60	90	
1.59	0.3	-	-	-	-	
	0.6	0.56	0.62	0.60	0.52(?)	
1.99	0.3	0.25	0.25	0.25	0.09 (?)	(First Shoulder)
	0.6	0.34	0.60	0.55	0.22(?)	
	1.2	0.44	1.05	1.20	1.12(?)	
2.49	0.3	0.28	0.12(?)	0.1 (?)	0.11(?)	(First Shoulder)
	0.6	0.28	0.64	0.52	0.54(?)	
	1.2	0.48	1.24	1.22	1.08(?)	
2.94	0.3	-	0.34	-	0.08(?)	(First Shoulder)
	0.6	-	-	0.66	0.36(?)	
	1.2	-	1.22	1.22	0.96(?)	

- denotes reattachment not clearly defined in flow visualization

(?) results are questionable(see text)

Reattachment Length Measured in Inches

TABLE 8

SEPARATION LENGTHS MEASURED FROM SHADOWGRAPHS

Mach Number	Step Height	Flare Angle α in Degrees 15	20	30	45	60	90	
1.59	0.3	0.095	0.325	0.665	0.933	1.12	≈1.33	(First Shoulder)
	0.6	0.156 0.119	0.265 0.245	0.82	1.63	1.87	2.37	
	1.2	0.115						
1.99	0.3	0.138 0.098	0.244	0.584 0.61	1.26	1.19	1.36	(First Shoulder)
	0.6	0.11	0.237	0.69	1.66	1.87	2.22	
	1.2	0.12	0.237	0.83	2.9	3.35	4.45	
2.49	0.3	0.076	0.134	0.52	0.845	1.09	1.23	(First Shoulder)
	0.6	≈0.01	0.047	0.47	1.47	1.9	2.3	
	1.2	≈0.02	0.16	0.845	2.68	3.46	4.3	
2.94	0.3	0.055	0.063	0.315	0.77	0.98	1.26	(First Shoulder)
	0.6	0.095	0.055	0.292	1.22	1.75	2.18	
	1.2	0.079	0.079	0.37	2.05	3.2	4.22	

Separation Length Measured in Inches

TABLE 9

SHOCK ANGLE IN DEGREES FROM SHADOWGRAPHS

Mach Number	Step Height	Flare Angle α in Degrees 15	20	30	45	60	90	
1.57	0.3	49.5	≈50	50.5	50	50	50	(First Shoulder)
	0.6	48.2 49.2	50.5 50.5	49.5	47.8	47.4	49.5	
	1.2	49.2						
1.99	0.3	40.5 41	42.2	40.2 41.5	37.9	40.0	41.4	(First Shoulder)
	0.6	40.9	40.5	40.7	37	40.0	40.4	
	1.2	39.9	40.6	39.6	38.5	38.8	39.5	
2.44	0.3	32.6	35.4	33.6	35.1	34.8	35.5	(First Shoulder)
	0.6	33.1	35.2	34.2	33.3	33.3	33.0	
	1.2	33.5	33.6	31.3	33.3	34.0	32.7	
2.87	0.3	28.2	32.9	29.6	30.0	29.4	29.0	(First Shoulder)
	0.6	27.7	32.0	29.8	29.6	28.5	29.8	
	1.2	28.0	31.8	30.2	29.5	~ 30	30.0	

TABLE 10

ANGLE BETWEEN LINE JOINING SEPARATION AND REATTACHMENT POINTS AND SURFACE

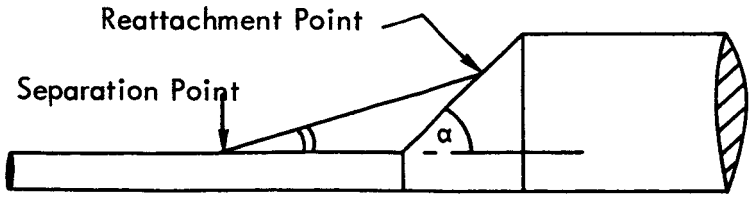

Mach Number	Step Height	Flare Angle α in Degrees 30	45	60	90
1.59	0.3	-	-	-	13
	0.6	12	13	14.5	15.5
1.99	0.3	9.5	10	12	15
	0.6	11.2	13	13.7	15
	1.2	10.2	13.3	15	16
2.49	0.3	11	(7)	(5.5)	14
	0.6	11.5	13.5	12	15
	1.2	11	13.3	14.5	15.5
2.94	0.3	-	13.7	16	13.3
	0.6	-	-	15.5	15
	1.2	-	16	15	16

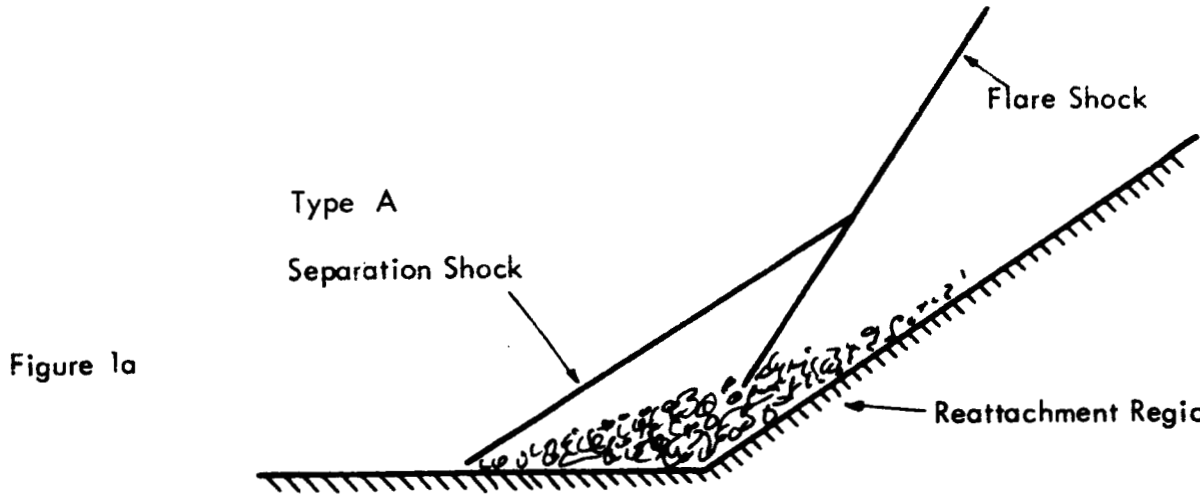

Figure 1a

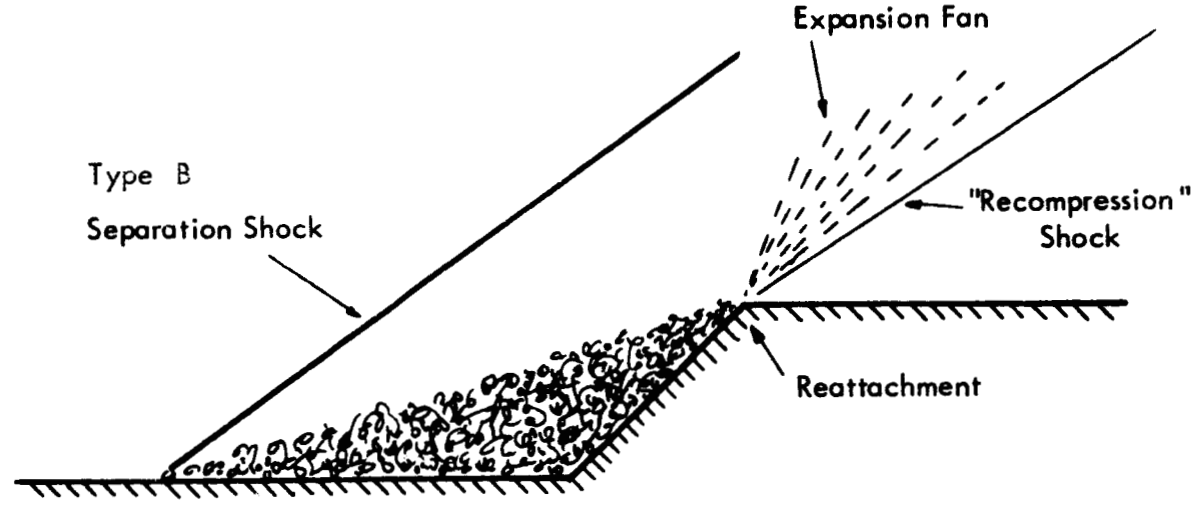

Figure 1b

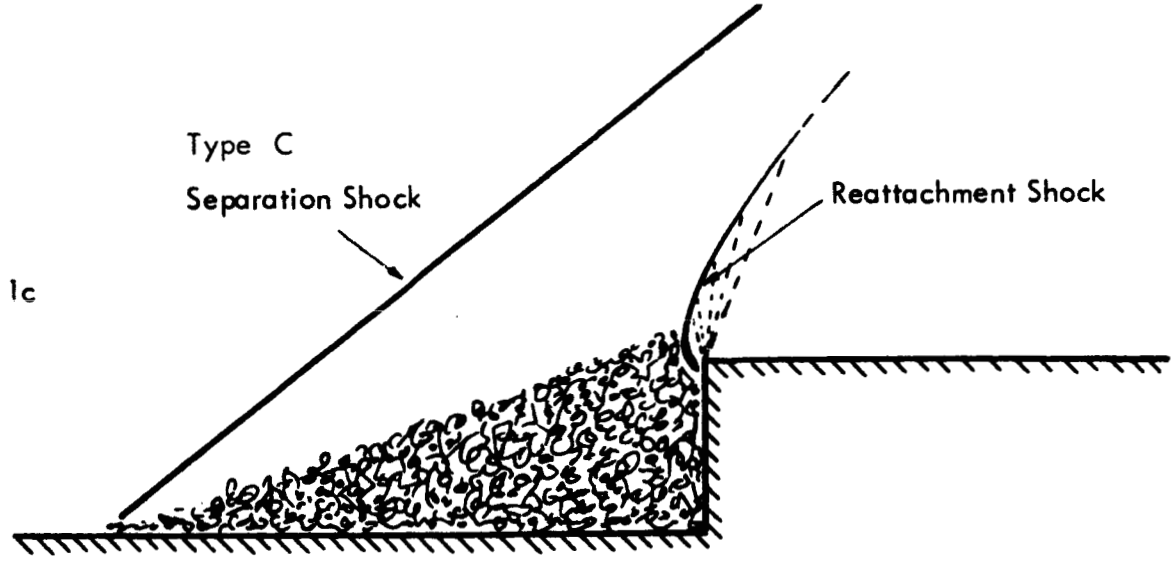

Figure 1c

Figure 1: Types of Turbulent Supersonic Separated Flow

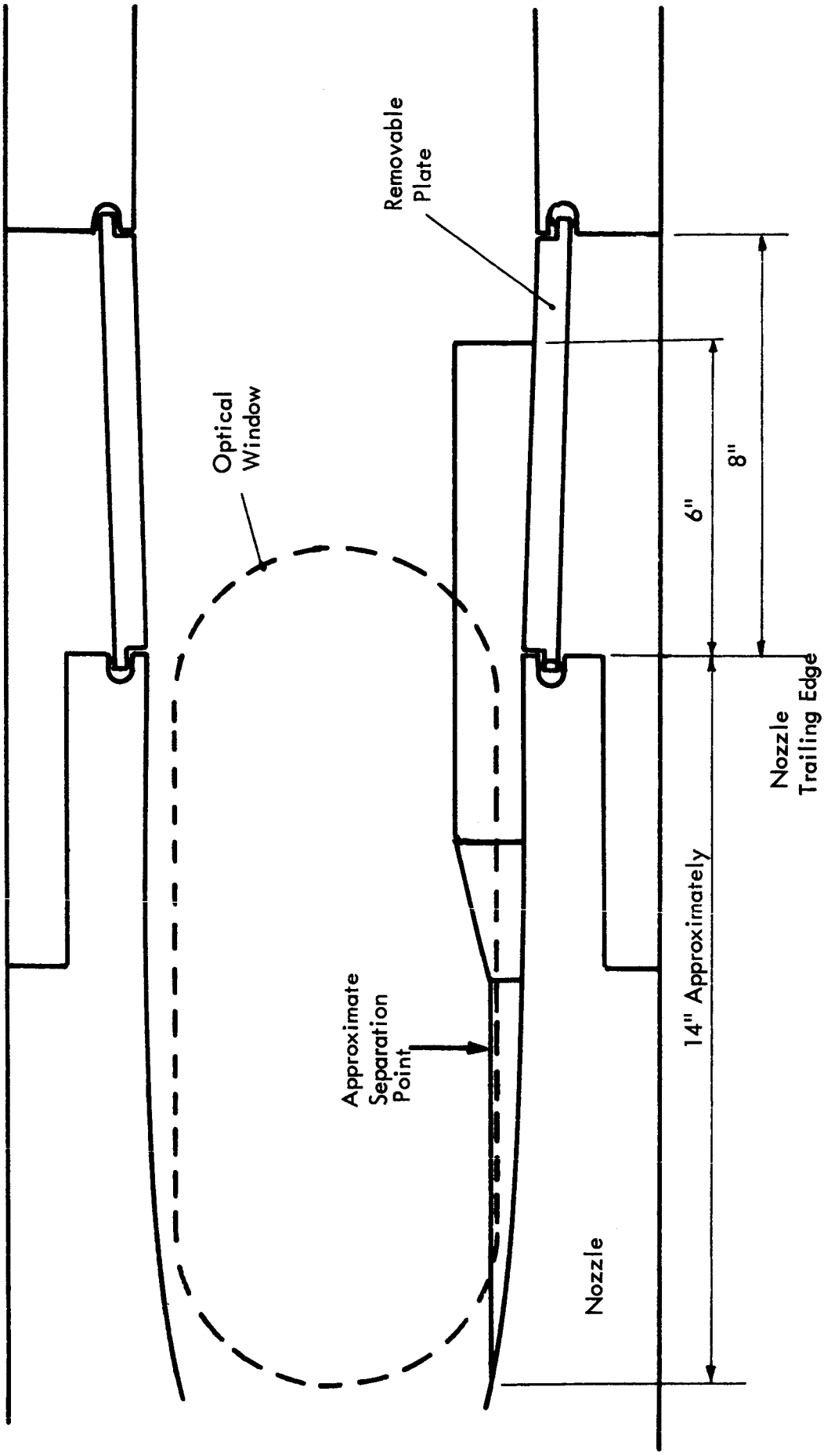

Figure 2: Sketch of Typical Half Model in 7" Tunnel.

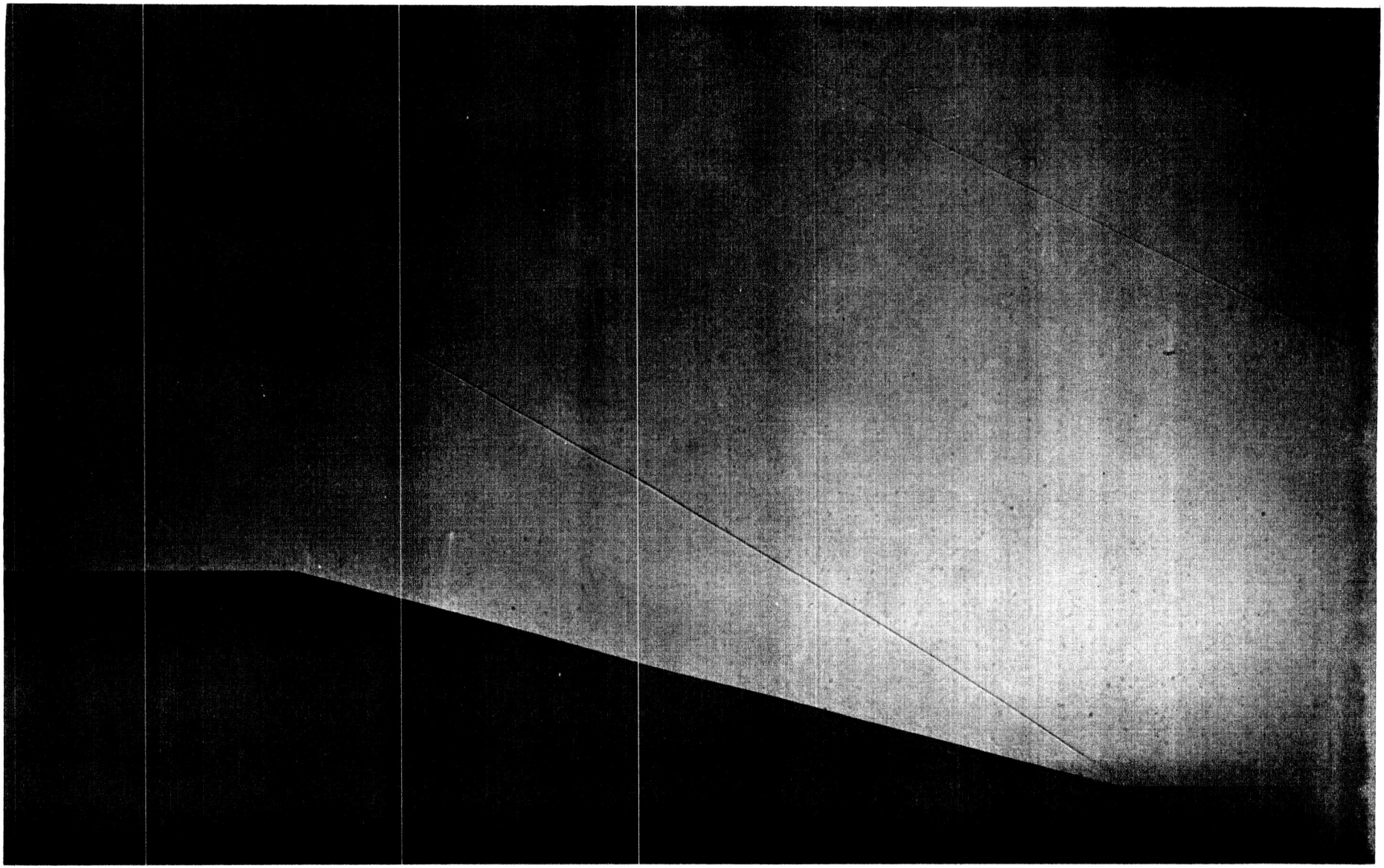

Figure 3. Shadowgraph of Flow at M = 2.49, Step Height = 1.2 inches.
Flare Angle = 15 degrees

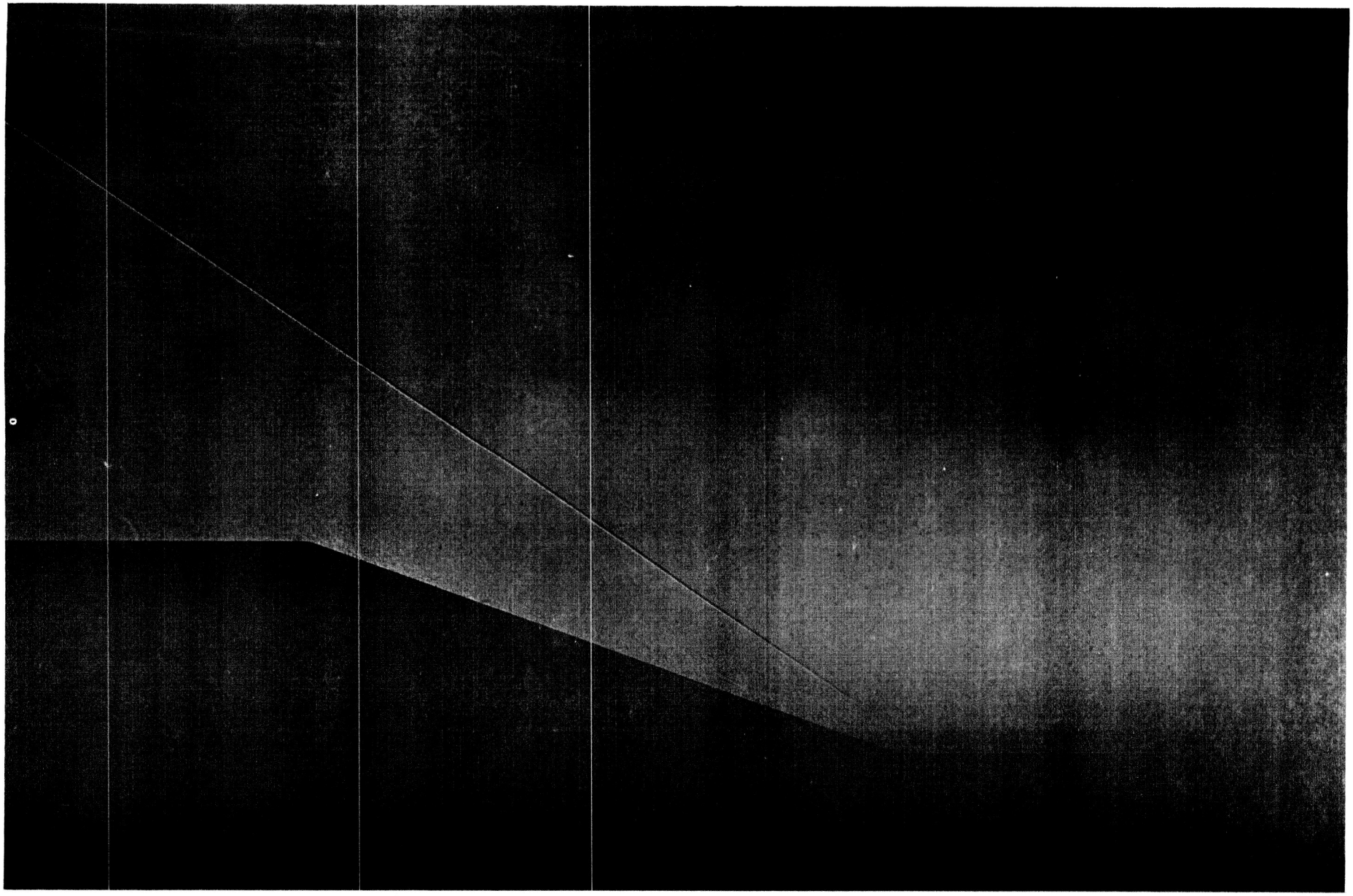

Figure 4. Shadowgraph of Flow at M = 2.49, Step Height = 1.2 inches.
Flare Angle = 20 degrees

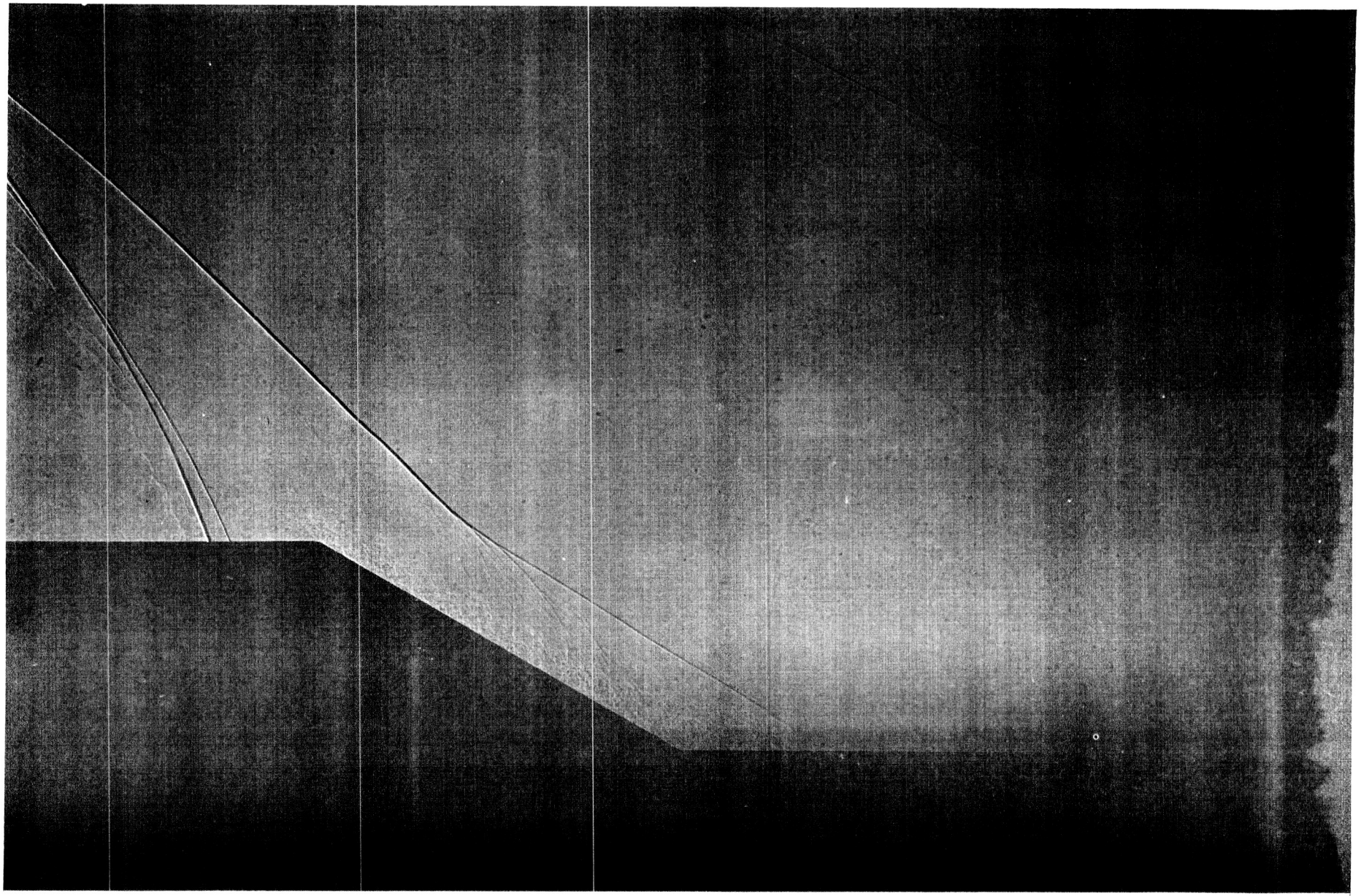

Figure 5. Shadowgraph of Flow at M = 2.49, Step Height = 1.2 inches.
Flare Angle = 30 degrees

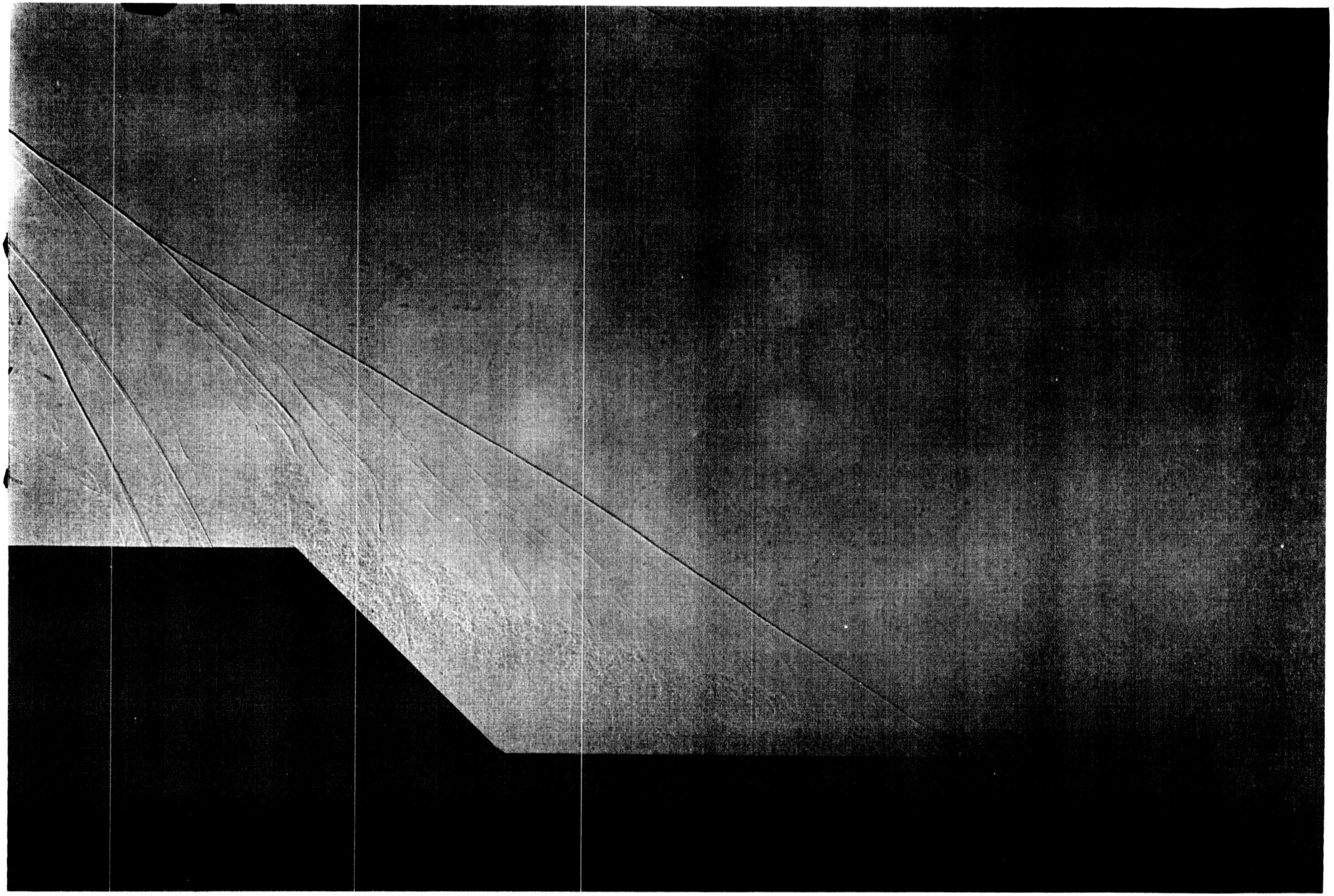

Figure 6. Shadowgraph of Flow at M = 2.49, Step Height = 1.2 inches.
Flare Angle = 45 degrees

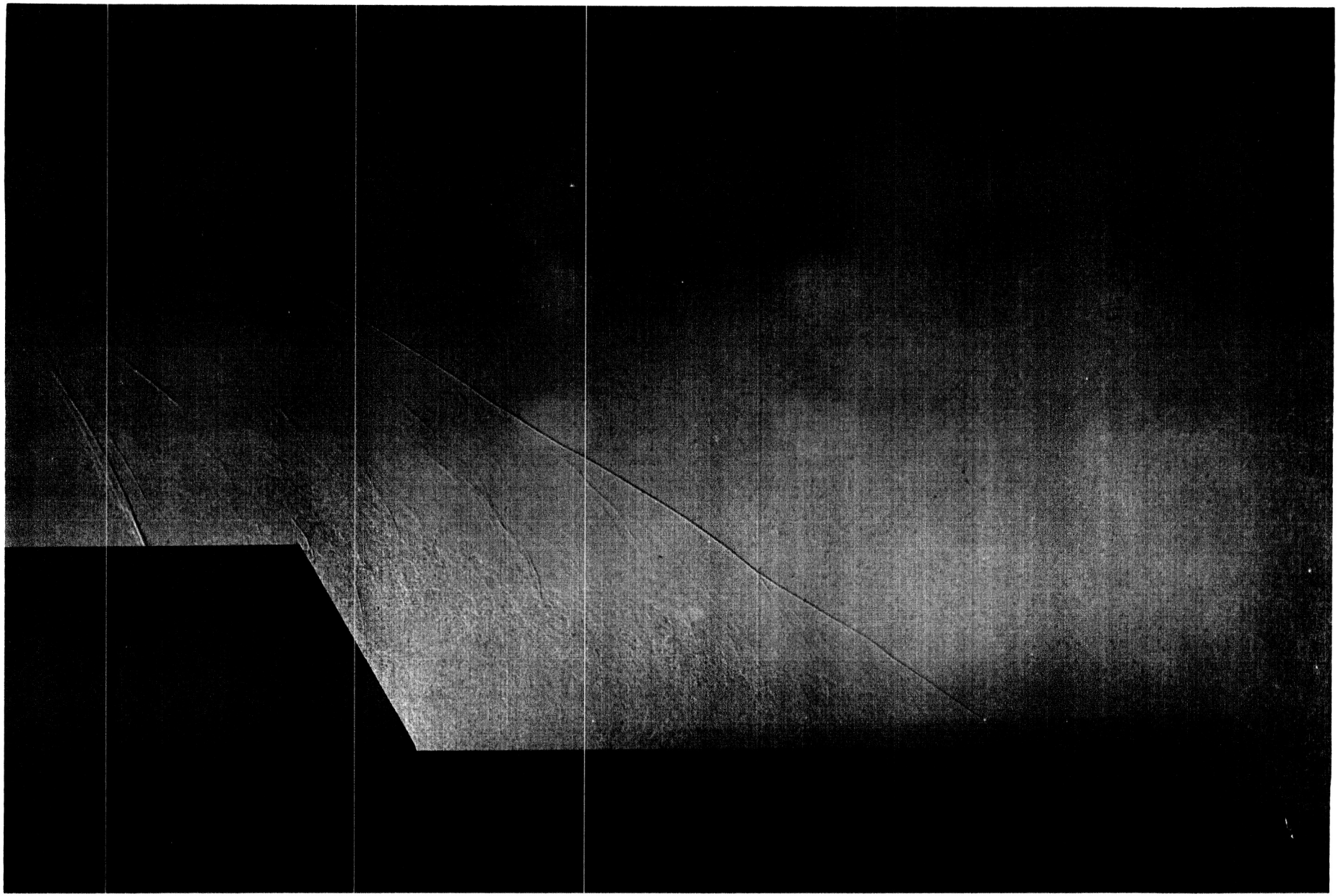

Figure 7. Shadowgraph of Flow at M = 2.49, Step Height = 1.2 inches.
Flare Angle = 60 degrees

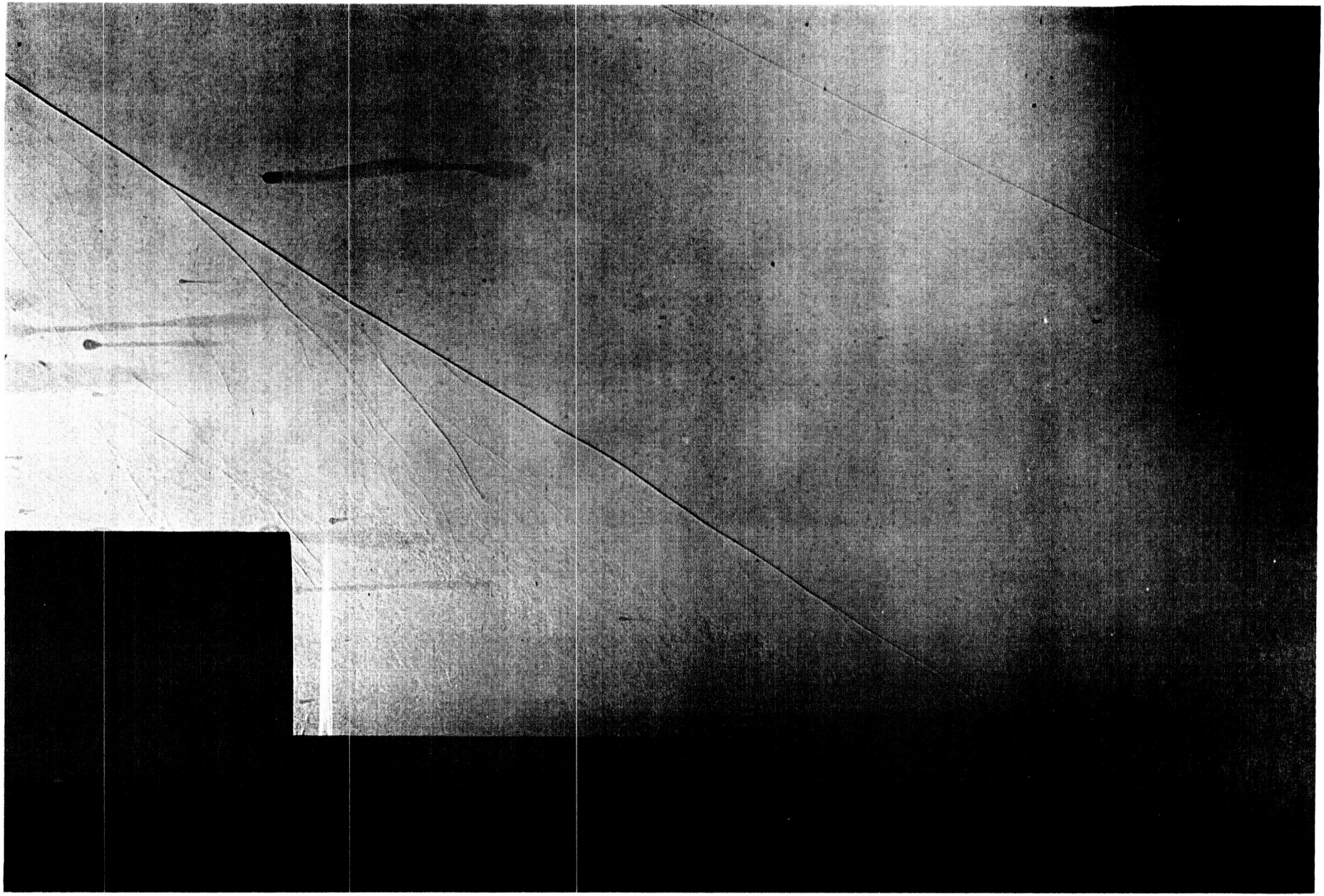

Figure 8. Shadowgraph of Flow at M = 2.49, Step Height = 1.2 inches.
Flare Angle = 90 degrees

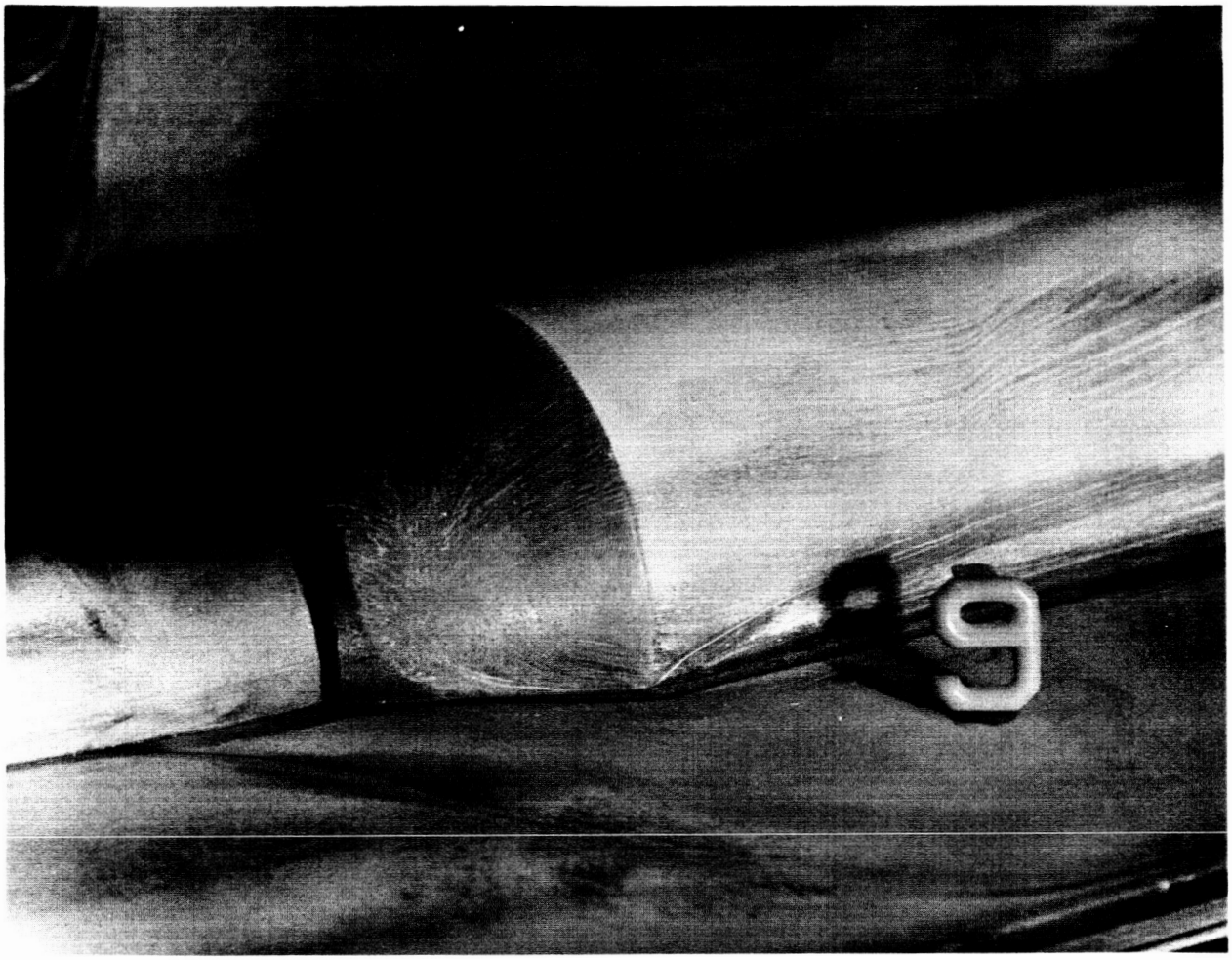

Figure 9. Surface Flow Visualization at M = 1.59, Step Height = 0.6 inch. Flare Angle = 30 degrees

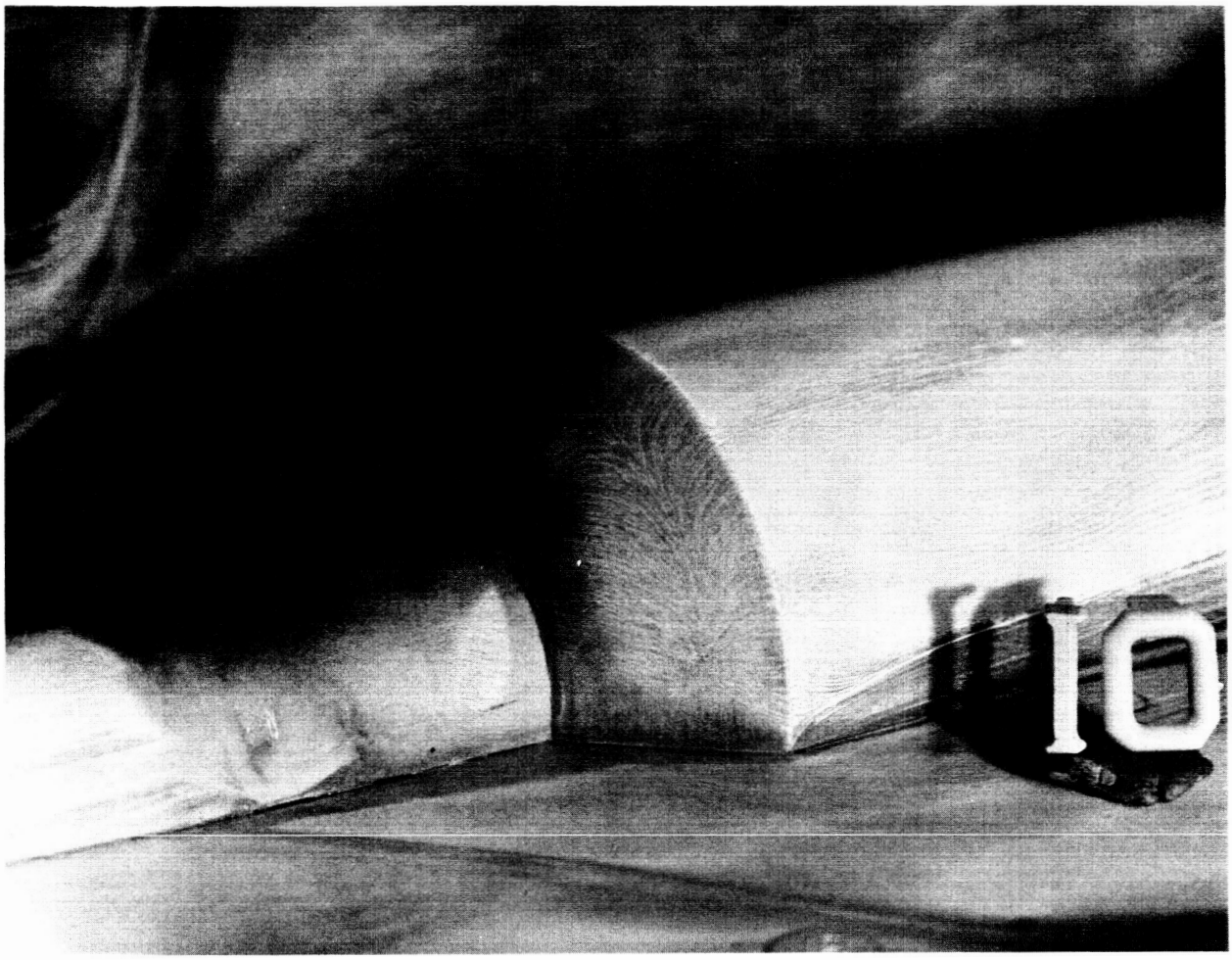

Figure 10. Surface Flow Visualization at M = 1.59, Step Height = 0.6 inch. Flare Angle = 45 degrees

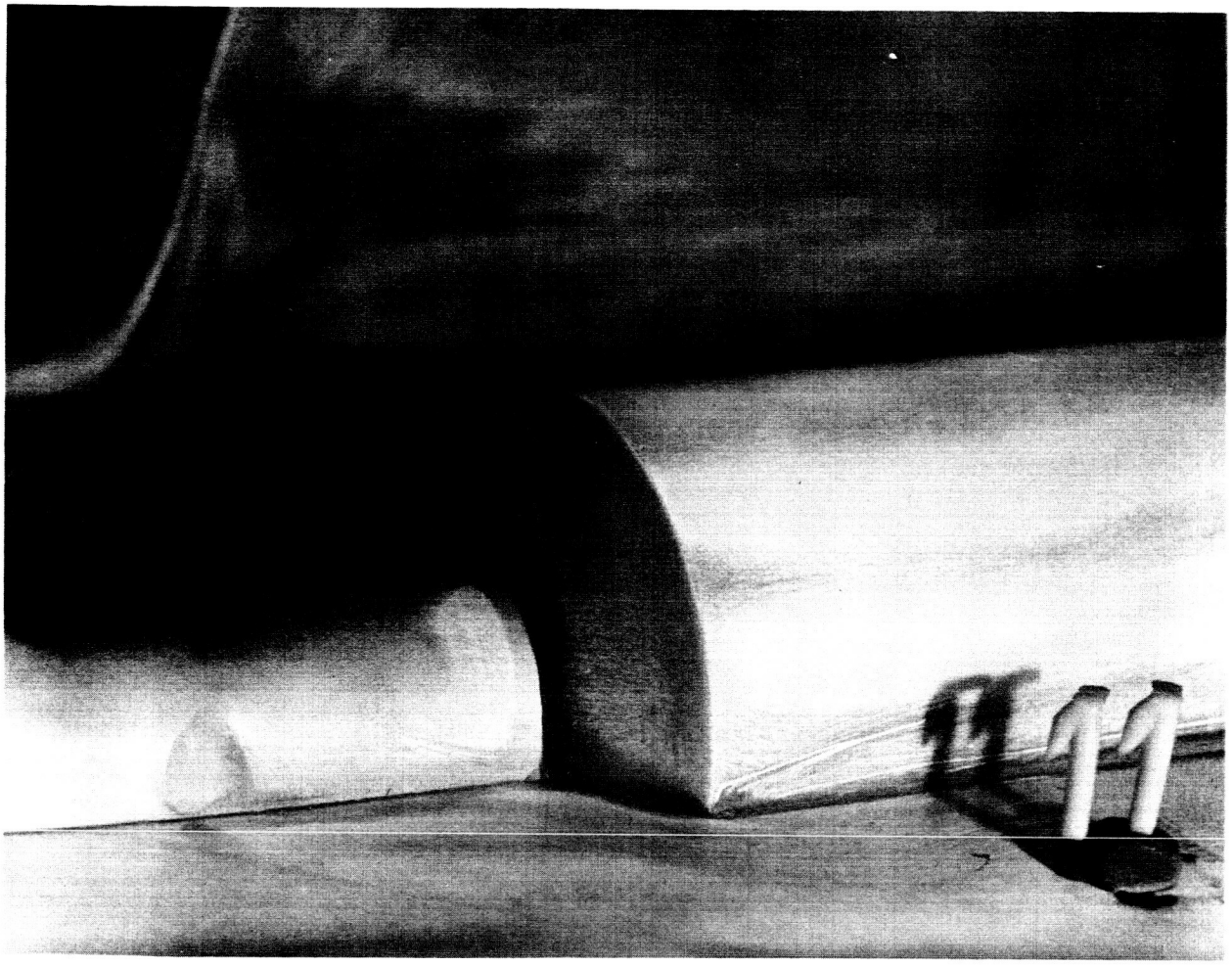

Figure 11. Surface Flow Visualization at M = 1.59, Step Height = 0.6 inch, Flare Angle = 60 degrees

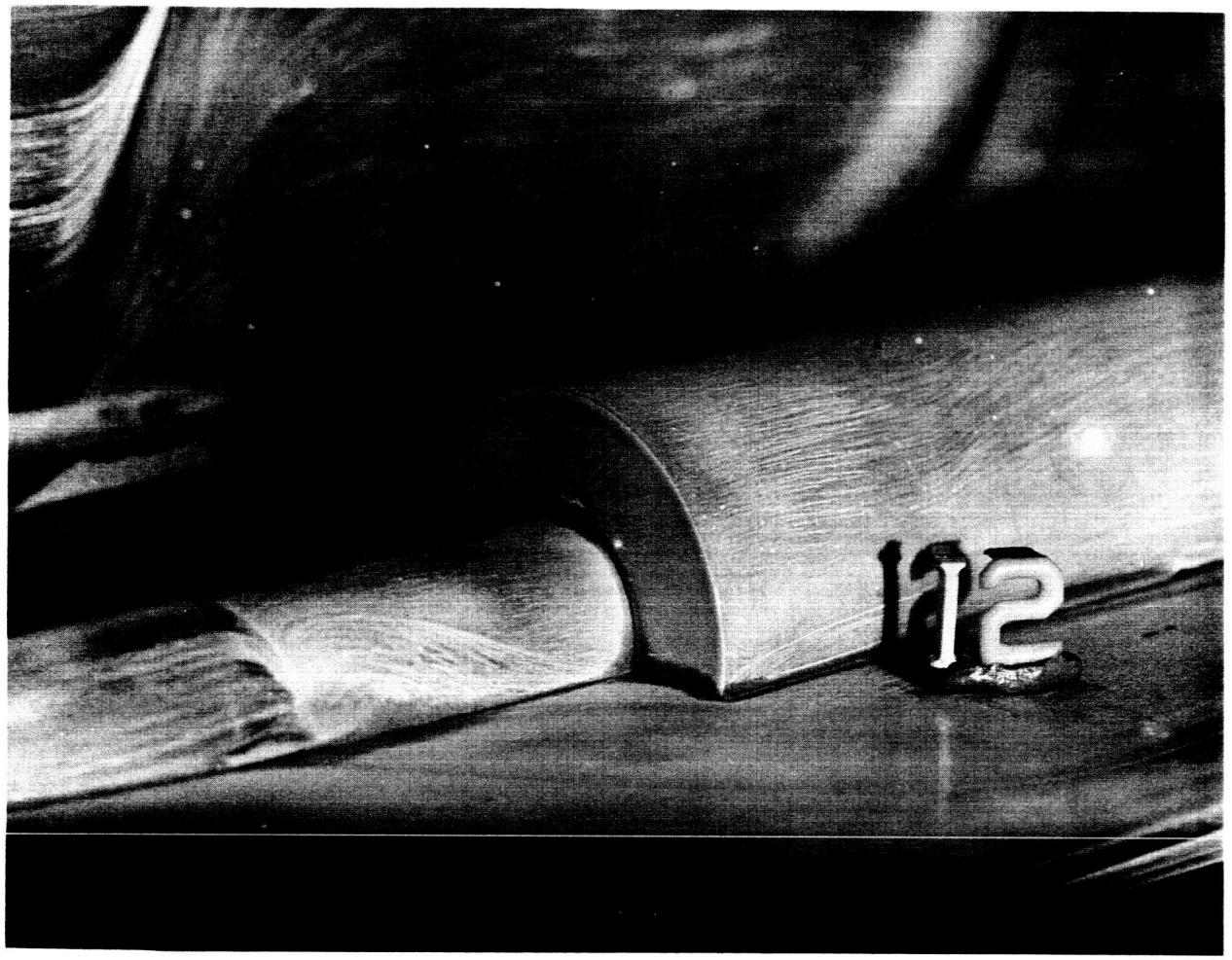

Figure 12. Surface Flow Visualization at M = 1.59, Step Height = 0.6 inch, Flare Angle = 90 degrees

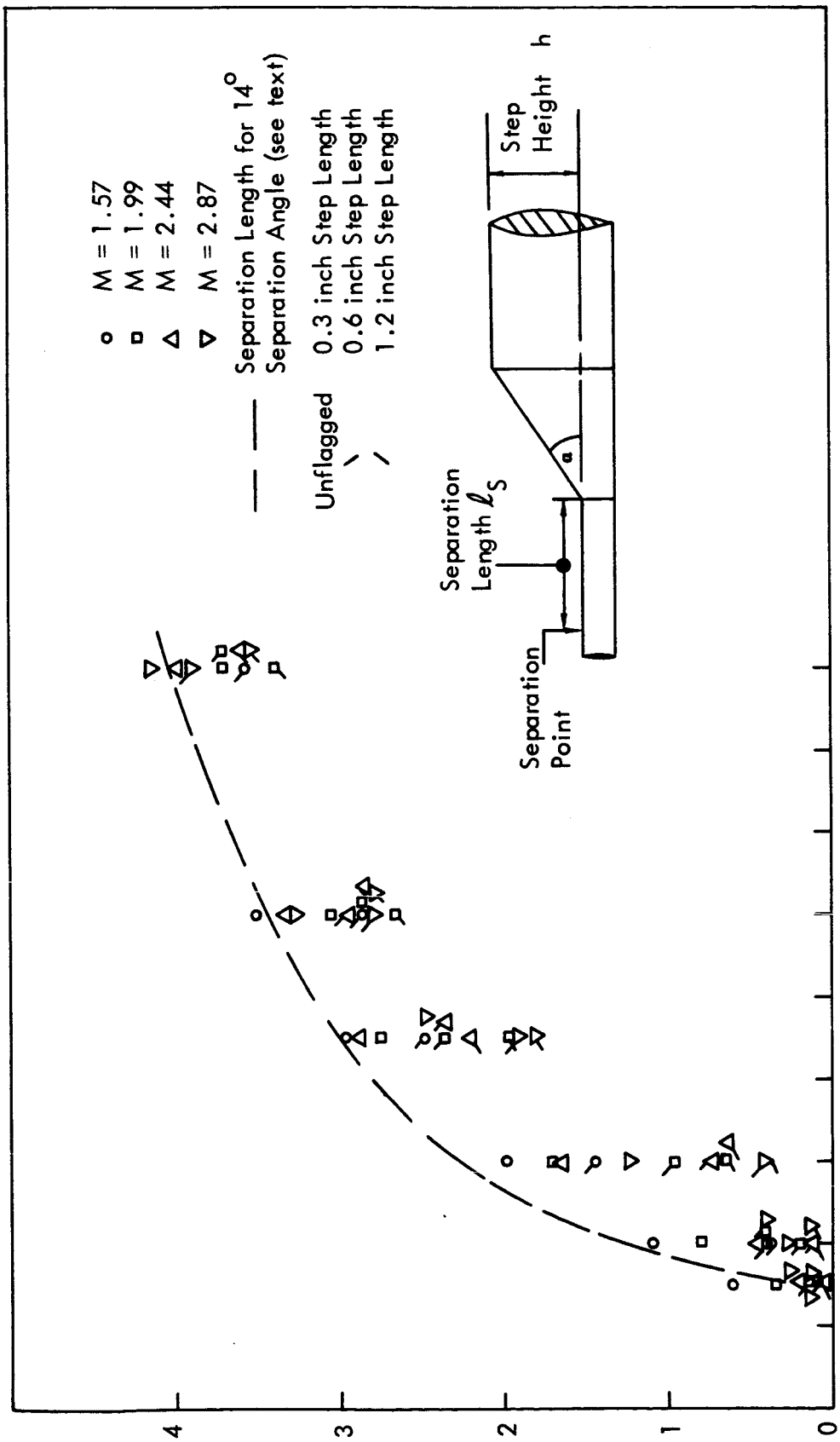

Figure 13. Separation Length vs Flare Angle from Surface Flow Visualization

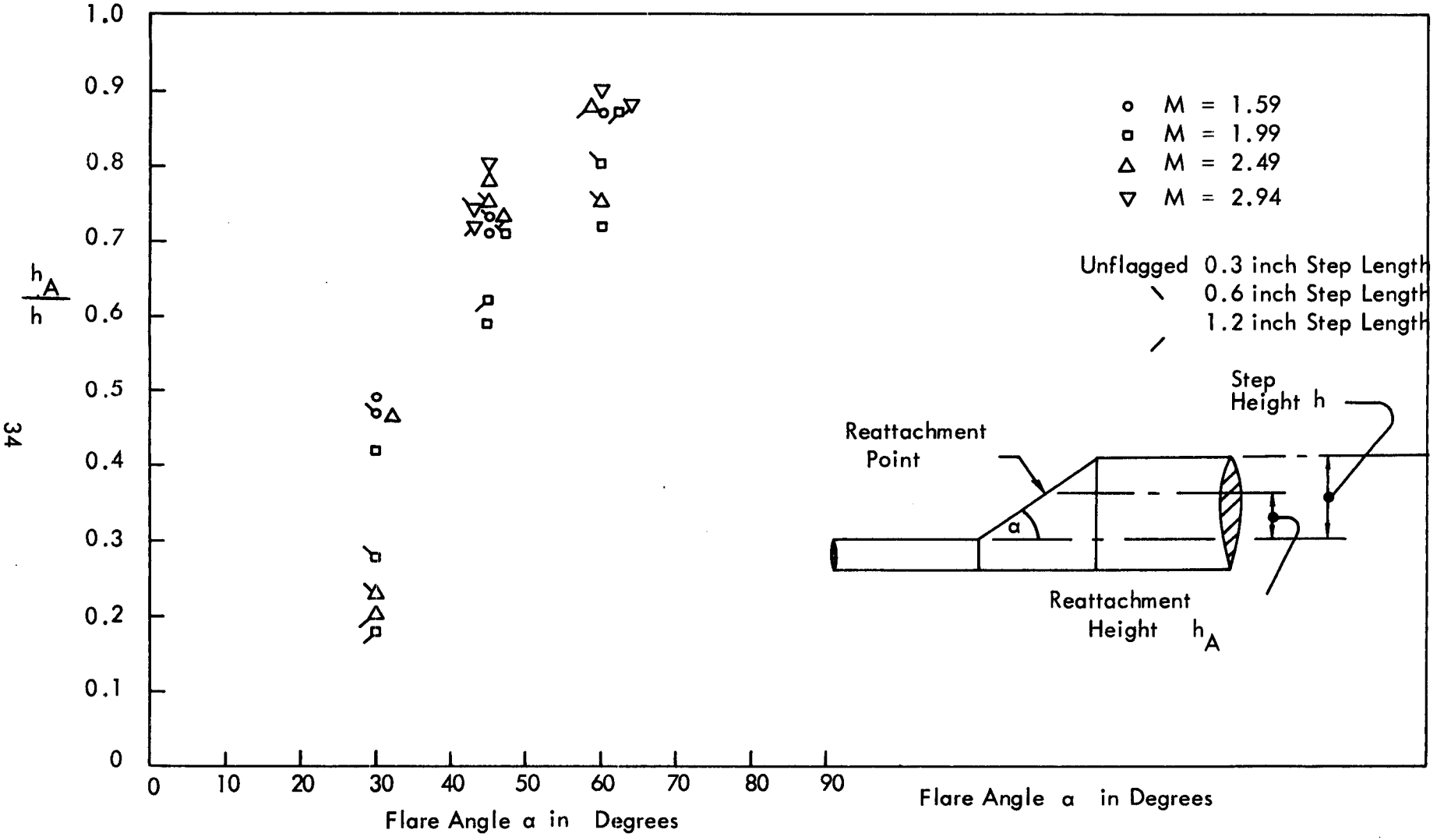

Figure 14. Non-Dimensionalized Reattachment Height vs Flare Angle from Surface Flow Visualization

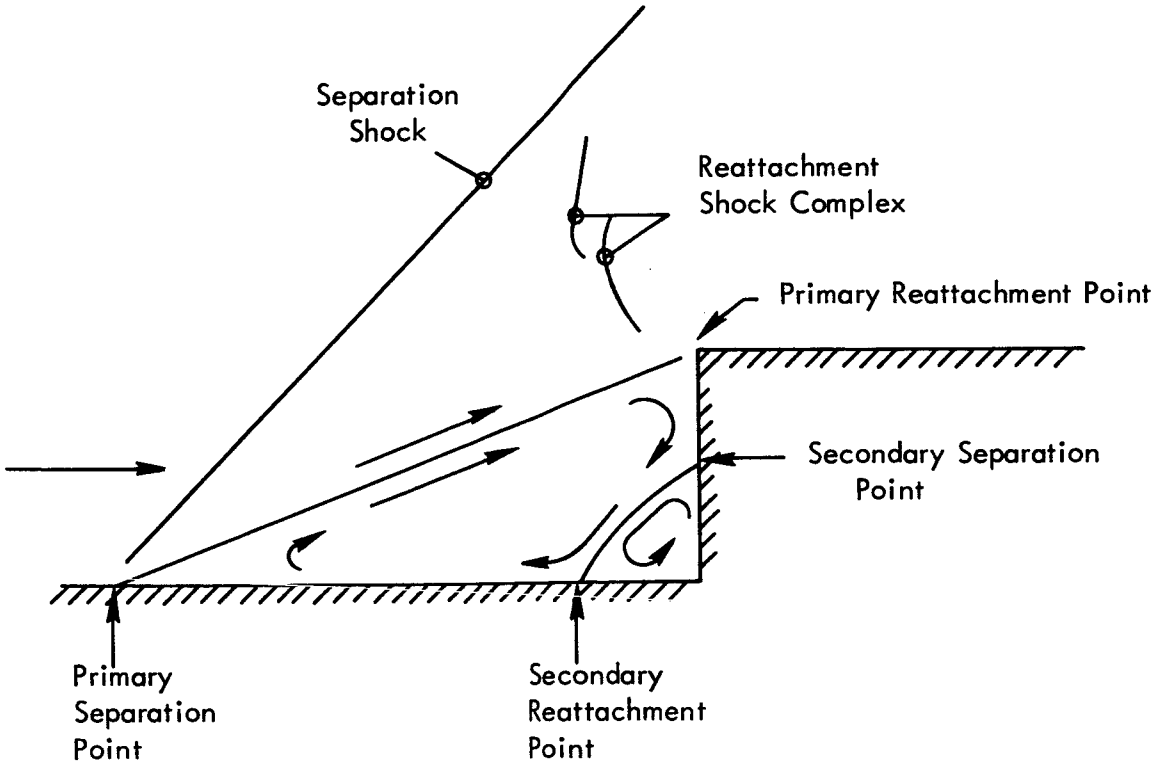

Figure 15. Possible Flow Pattern with Secondary Separation at High Flare Angles.

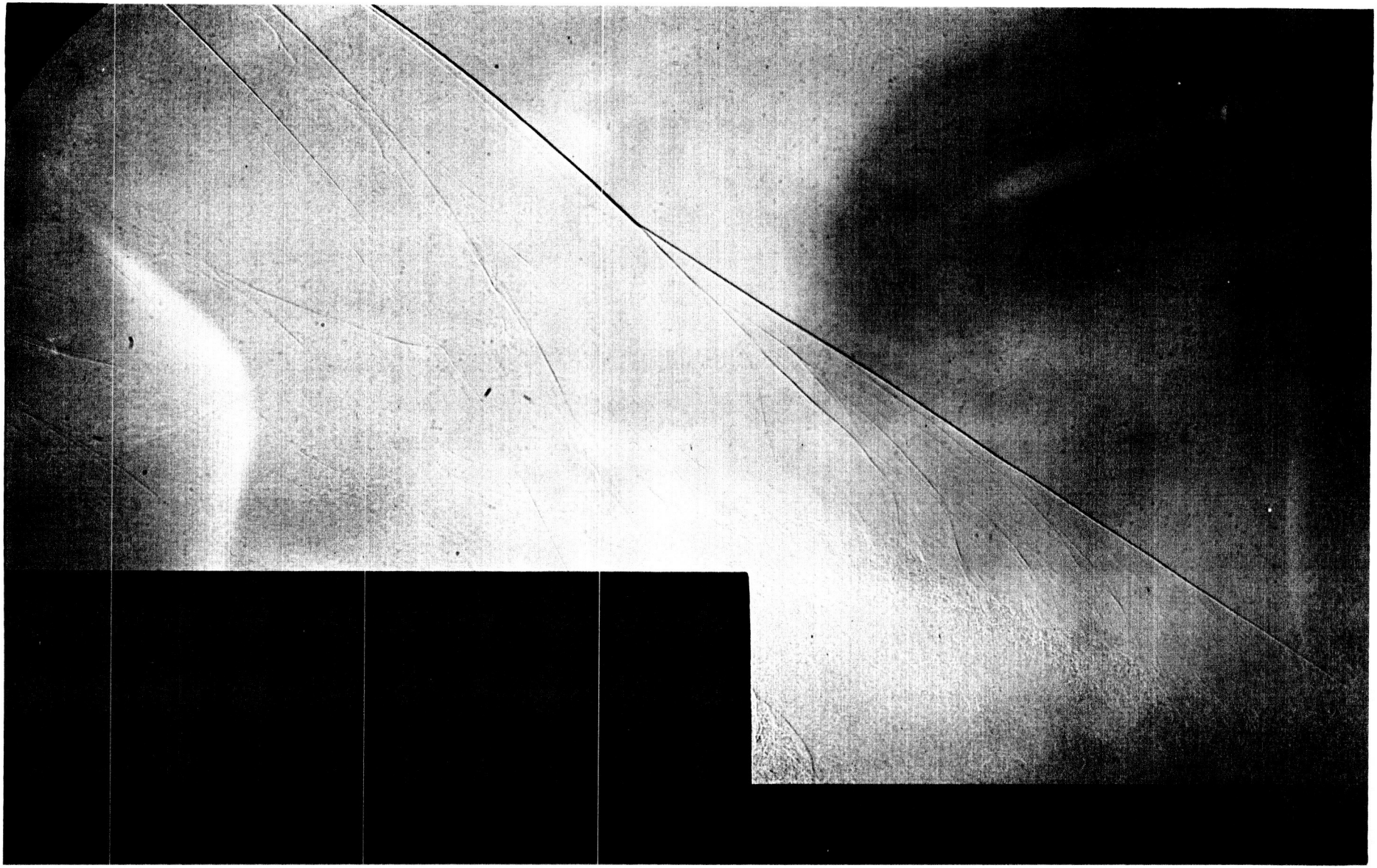

Figure 16. Shadowgraph of Flow at M = 2.49, Step Height = 1.2 inches.
Flare Angle = 90 degrees
Compare to Figures 17, 18, and 8)

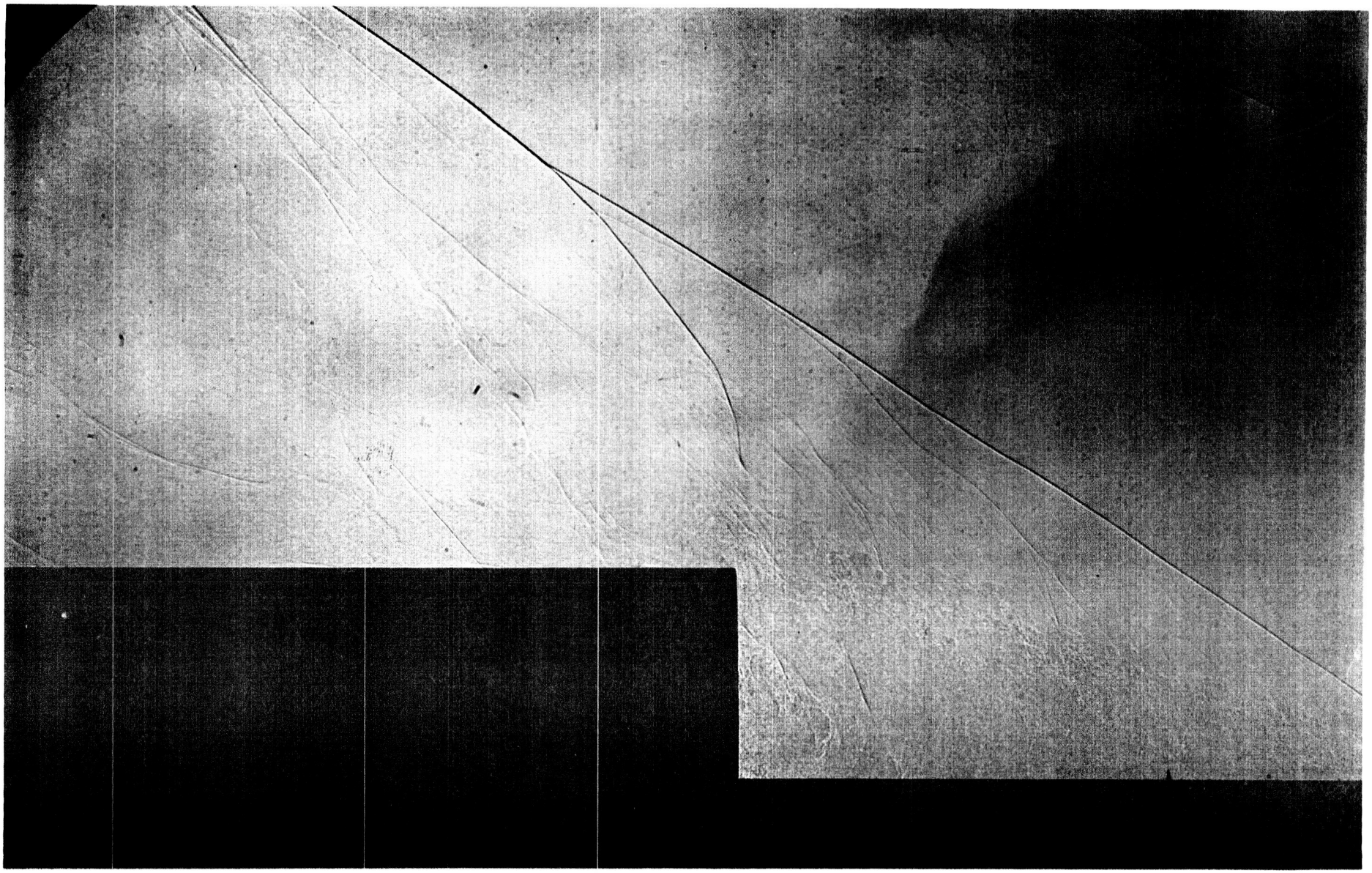

Figure 17. Shadowgraph of Flow at M = 2.49, Step Height = 1.2 inches.
Flare Angle = 90 degrees
(Compare to Figures 16, 18, and 8)

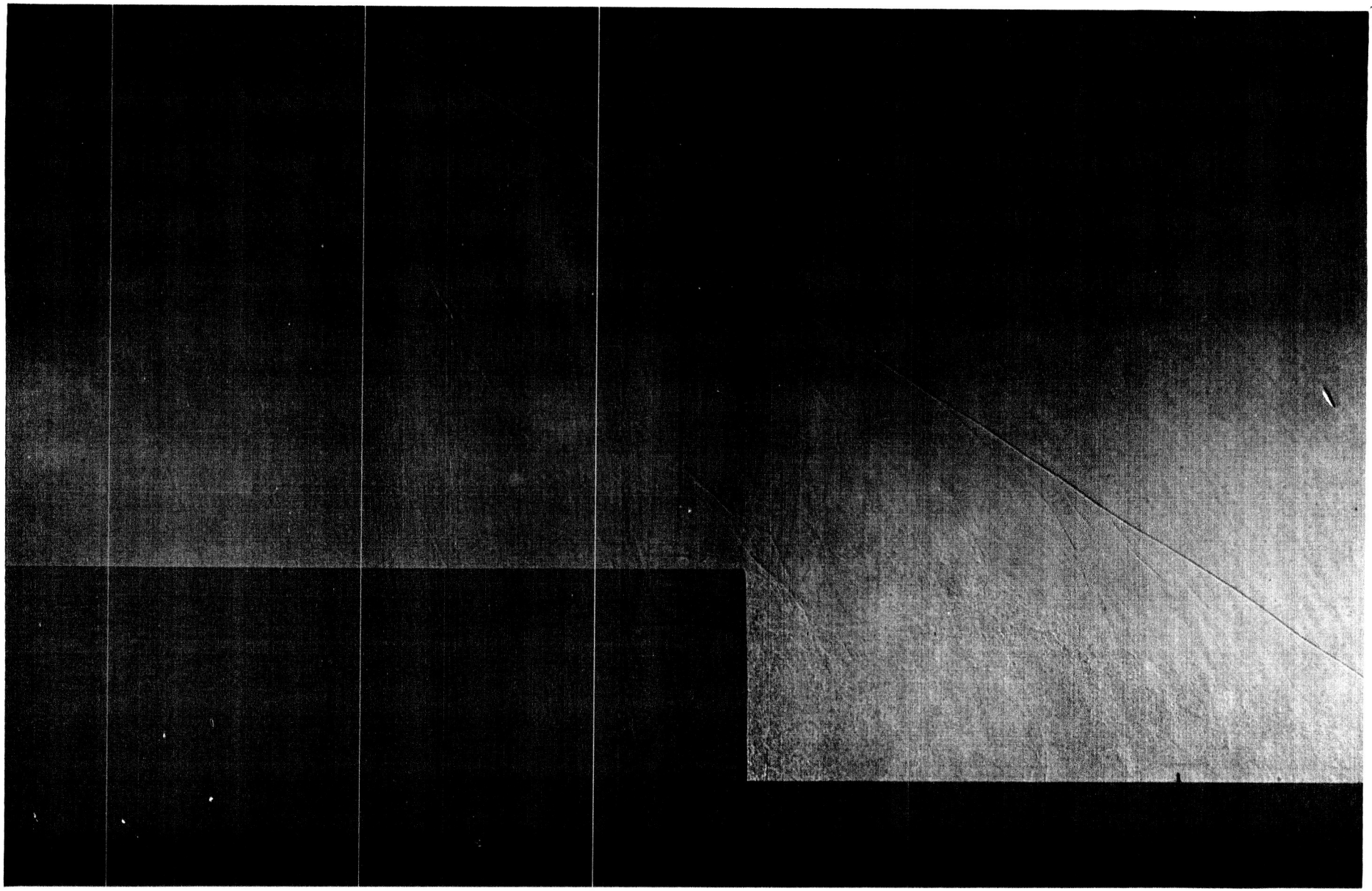

Figure 18. Shadowgraph of Flow at M = 2.49, Step Height = 1.2 inches.
Flare Angle = 90 degrees
(Compare to Figures 16, 17, and 8)